

Supporting Information

Self-Assembly of Two-Dimensional Bimetallic Nickel-Cobalt Phosphate Nanoplates into One-Dimensional Porous Chain-Like Architecture for Efficient Oxygen Evolution Reaction

Ni Luh Wulan Septiani¹, Yusuf Valentino Kaneti^{2*}, Kresna Bondan Fathoni¹, Kenya Kani³, Abeer Enaiet Allah⁴, Brian Yulianto^{1,5*}, Nugraha^{1,5}, Hermawan Kresno Dipojono^{1,5}, Zeid A. Alothman,⁶ Dmitri Golberg^{2,7,8*} and Yusuke Yamauchi^{3,9*}

1 Department of Engineering Physics, Institute of Technology Bandung (ITB), Bandung 40132, Indonesia

2 International Center for Materials Nanoarchitectonics (WPI-MANA), National Institute for Materials Science (NIMS), 1-1 Namiki, Tsukuba, Ibaraki 305-0044, Japan

3 School of Chemical Engineering and Australian Institute for Bioengineering and Nanotechnology (AIBN), The University of Queensland, Brisbane, QLD 4072, Australia

4 Department of Chemistry, Faculty of Science, Beni-Suef University, Beni-Suef 62511, Egypt

5 Research Center for Nanosciences and Nanotechnology (RCNN), Institute of Technology Bandung (ITB), Bandung 40132, Indonesia

6 Chemistry Department, College of Science, King Saud University, Riyadh 11451, Saudi Arabia

7 Centre for Materials Science, Queensland University of Technology, 2 George str., Brisbane, QLD 4000, Australia

8 School of Chemistry and Physics, Science and Engineering Faculty, Queensland University of Technology, 2 George str., Brisbane, QLD 4000, Australia

9 Department of Plant and Environmental New Resources, Kyung Hee University, 1732 Deogyong-daero, Giheung-gu, Yongin-si, Gyeonggi-do, 446-701, South Korea

E-mails: KANETI.Valentino@nims.go.jp; brian@tf.itb.ac.id; y.yamauchi@uq.edu.au;

dmitry.golberg@qut.edu.au

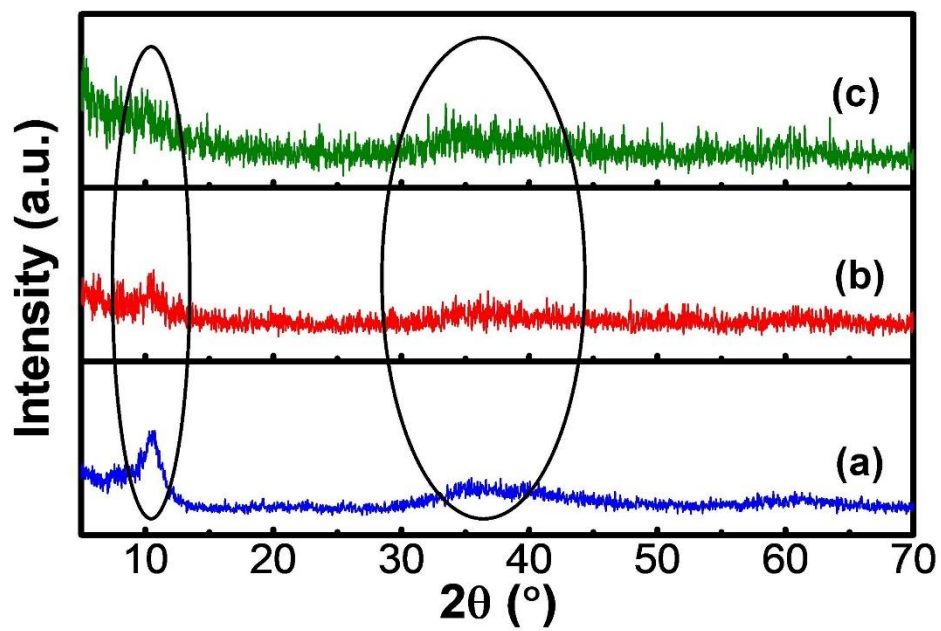


Figure S1. X-ray diffraction (XRD) patterns of (a) cobalt glycerate, (b) nickel-cobalt glycerate, and (c) nickel glycerate.

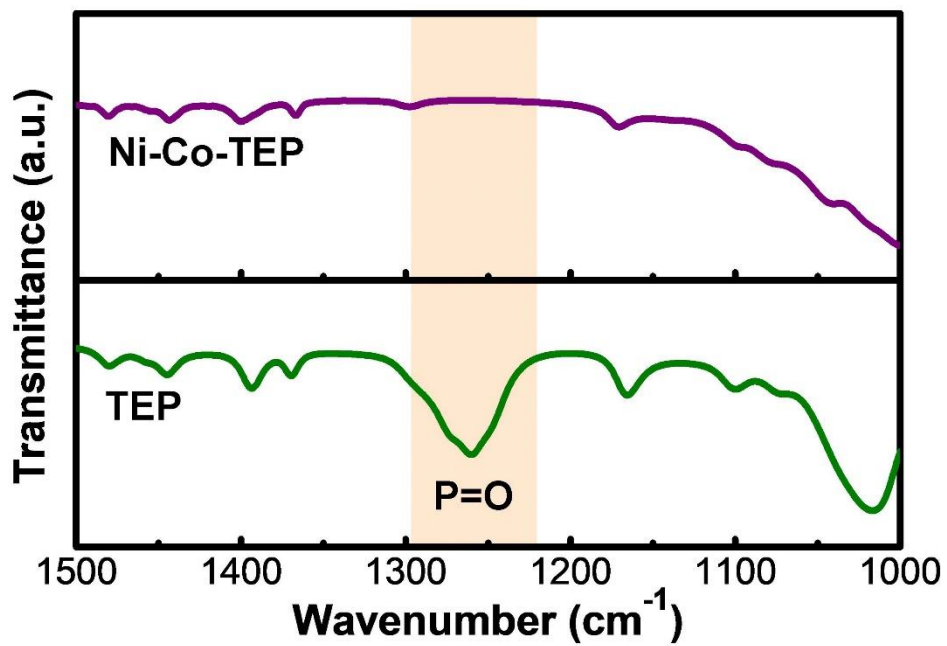


Figure S2. Comparison of FTIR spectra of TEP and Ni-Co-TEP showing the disappearance of P=O band at 1297 cm⁻¹ due to the transformation of triethyl phosphate (TEP) to diethyl phosphate (DEP).

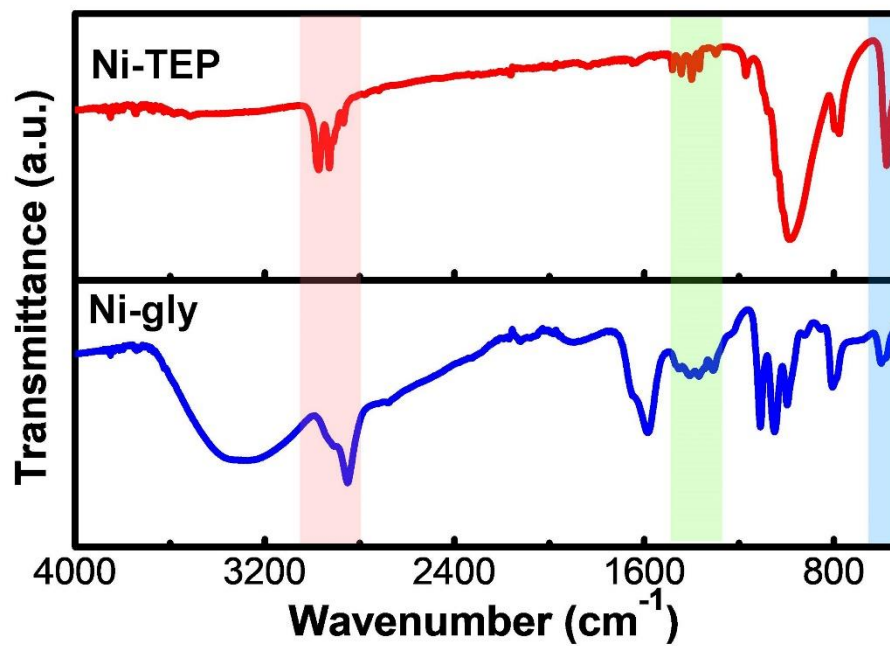


Figure S3. Comparison of FTIR spectra of nickel glycerate and Ni-TEP.

Table S1. The molar ratios of Ni, Co, and P for Ni-TEP, Co-TEP, and NiCo-TEP samples as measured by ICP-OES.

Sample	<i>n</i> (Ni/P)	<i>n</i> (Co/P)
Ni-TEP	1.04	0
Co-TEP	0	1.15
NiCo-TEP	0.67	0.39

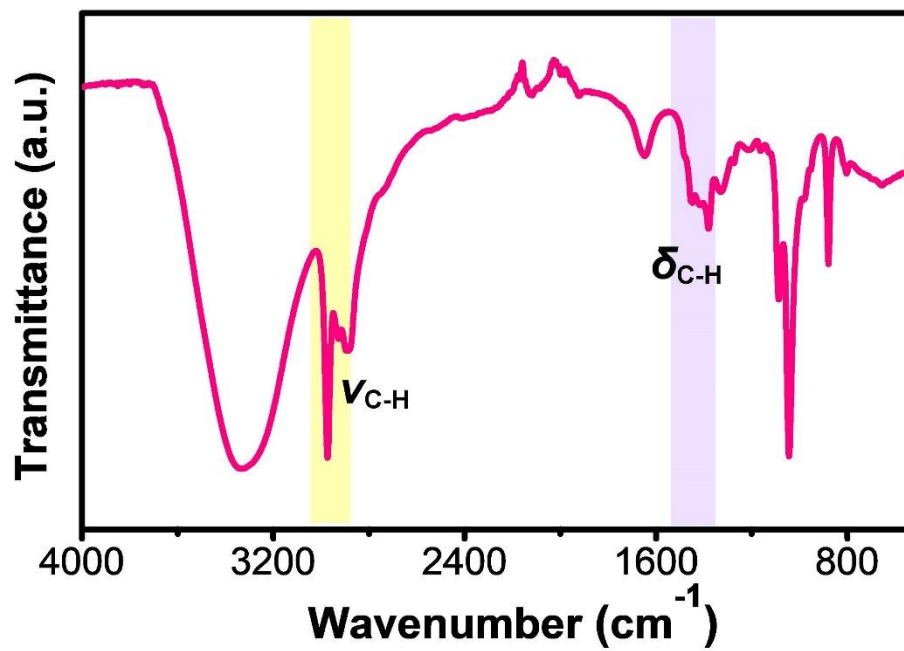


Figure S4. FTIR spectrum of the supernatant collected after the solvothermal reaction between Ni-Co glycerate and TEP in ethanol at 180 °C for 16 h.

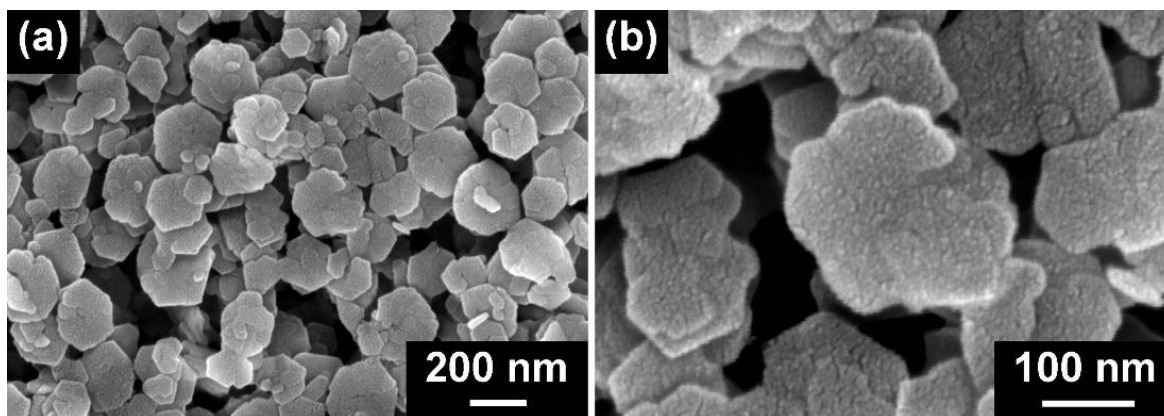


Figure S5. (a) Low- and (b) high-magnification SEM images of the product obtained using $\text{Ni}(\text{NO}_3)_2 \cdot 6\text{H}_2\text{O}$ and $\text{Co}(\text{NO}_3)_2 \cdot 6\text{H}_2\text{O}$ as Ni and Co sources and TEP at 180 °C for 16 h.

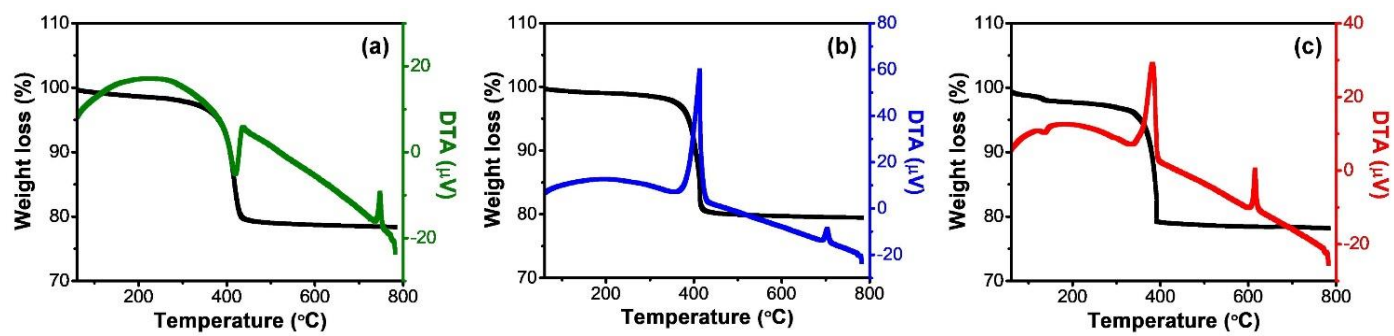


Figure S6. TG-DTA curves of Ni-TEP (a), Ni-Co-TEP (b), and Co-TEP (c) from room temperature to 800 °C at a heating rate of 10 °C/min under air atmosphere.

Table S2. Crystallographic data of CoP₂O₇ according to ICSD No. 84-2126

2θ	hkl	d-spacing	Relative intensity
13.80	100	6.412	39
15.10	011	5.863	21
17.30	$\bar{1}11$	5.122	35
17.43	110	5.084	84
20.37	$\bar{1}02$	4.356	81
21.28	020	4.172	16
21.56	002	4.118	46
23.01	$\bar{1}12$	3.862	12
23.31	111	3.813	78
23.89	021	3.722	16
24.08	012	3.693	32
25.36	$\bar{1}21$	3.509	31
27.59	$\bar{2}11$	3.230	8
27.81	200	3.205	9
29.53	$\bar{2}12$	3.022	581
29.62	$\bar{1}22$	3.014	1000
29.86	210/121	2.990	94
30.14	$\bar{1}02$	2.963	613
30.47	022	2.931	26
31.67	$\bar{1}13$	2.823	52
32.03	112	2.792	3
33.37	$\bar{2}21$	2.683	22
33.99	031	2.635	14
34.36	013	2.608	34
35.14	130	2.552	170
35.28	220	2.542	228
35.55	211	2.523	23
36.87	$\bar{1}23$	2.436	1
37.19	122	2.416	12
38.36	$\bar{1}32$	2.345	1
38.55	131	2.334	3
38.82	$\bar{3}02$	2.318	24
39.05	032	2.305	25
39.84	$\bar{2}23$	2.261	1
40.19	$\bar{1}04$	2.242	5
40.32	221/ $\bar{3}12$	2.235	14
40.53	$\bar{3}11$	2.224	5
41.42	$\bar{2}31/\bar{2}04$	2.178	21
41.68	$\bar{1}14$	2.165	23
42.09	113/202	2.145	92
42.26	300	2.137	53
42.79	$\bar{2}32$	2.112	217
42.87	$\bar{2}14$	2.108	123
43.34	040	2.086	5
43.55	212	2.076	46
43.70	310	2.070	54
43.94	004	2.059	22

44.37	133	2.040	7
44.69	132/322	2.026	63
44.85	041/321	2.019	38
45.33	014	1.999	1
45.64	141/140	1.986	4
45.92	124	1.975	7
46.29	123	1.960	1
46.44	033	1.954	5
47.02	224	1.931	19
47.37	323/231	1.918	9
47.65	222	1.907	3
47.79	320	1.902	7
48.33	142	1.882	24
48.49	141	1.876	19
48.61	314	1.872	9
49.32	024/311	1.846	80
50.90	241	1.793	3
51.26	332	1.781	3
51.41	331	1.776	3
51.79	104	1.764	9
52.17	402	1.752	8
52.37	134/324	1.746	30
52.72	133	1.735	6
53.14	321	1.722	56
53.40	412	1.714	17
53.69	333/142	1.706	21
53.95	232	1.698	37
54.08	330	1.694	48
54.45	413	1.684	6
54.83	411	1.673	6
55.26	043	1.661	6
55.71	243	1.649	10
55.90	302/225	1.643	8
56.08	315/241	1.639	12
56.19	051/125	1.636	33
56.72	404	1.622	73
56.97	015/150	1.615	96
57.46	400	1.603	17
58.34	421/334	1.580	130
59.02	331	1.564	4
59.24	152	1.559	3
59.53	325/342	1.552	13
59.74	341/052	1.547	28
60.47	322	1.530	20
60.58	144	1.527	11
60.89	143	1.520	2
61.28	424	1.511	11
61.49	251/224	1.507	8
61.79	206	1.500	3
61.98	420/242	1.496	8

62.13	340	1.493	5
62.28	134/233	1.490	7
62.62	$\bar{4}32/204$	1.482	62
63.24	$\bar{1}06$	1.469	4
63.42	044/ $\bar{4}15$	1.466	25
63.57	$\bar{4}33$	1.462	13
63.76	$\bar{1}53/214$	1.459	5
63.91	$\bar{4}31/152$	1.455	4

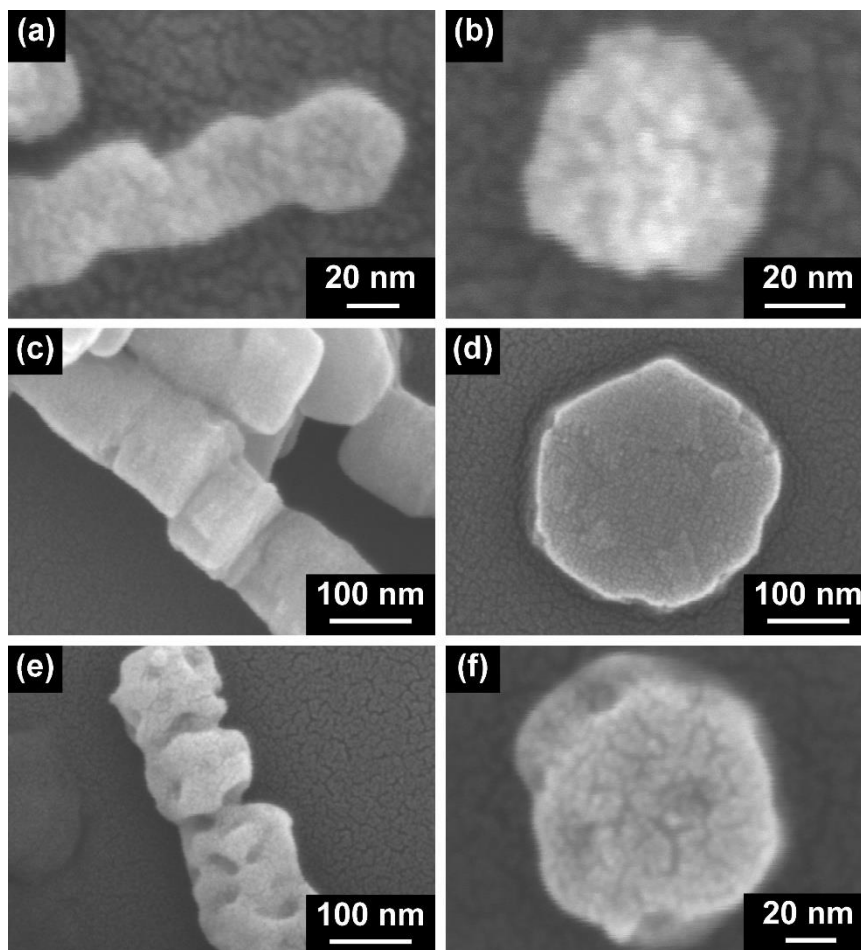


Figure S7. SEM images showing a single chain-like Ni-TEP-600 (amorphous nickel phosphate) particle (a) and a single porous hexagonal nanoplate assembling the chain-like Ni-TEP-600 particle (b). SEM images of a single chain-like Ni-Co-TEP particle (c) and the hexagonal nanoplate assembling the chain-like Ni-Co-TEP particle (before calcination) (d). SEM images of a single chain-like Ni-Co-TEP-600 particle (e) and a single nanoplate assembling the porous chain-like Ni-Co-TEP-600 particle (f), showing slightly distorted hexagonal-like morphology with rough surface texture.

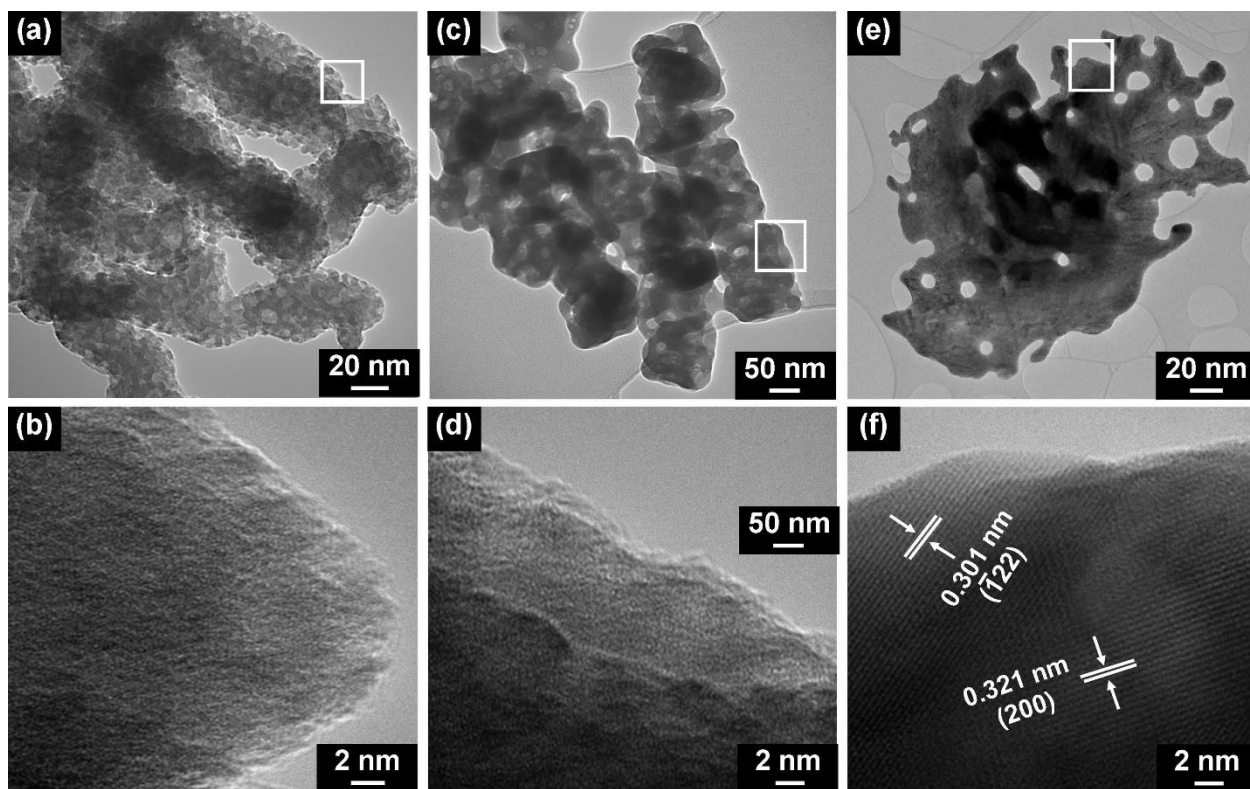


Figure S8. TEM and high-resolution TEM (HRTEM) images of Ni-TEP-600 (a, b), Ni-Co-TEP-600 (c, d), and Co-TEP-600 (e, f) taken from the areas inside the white rectangles of **Figures S8a, c, and e**, respectively.

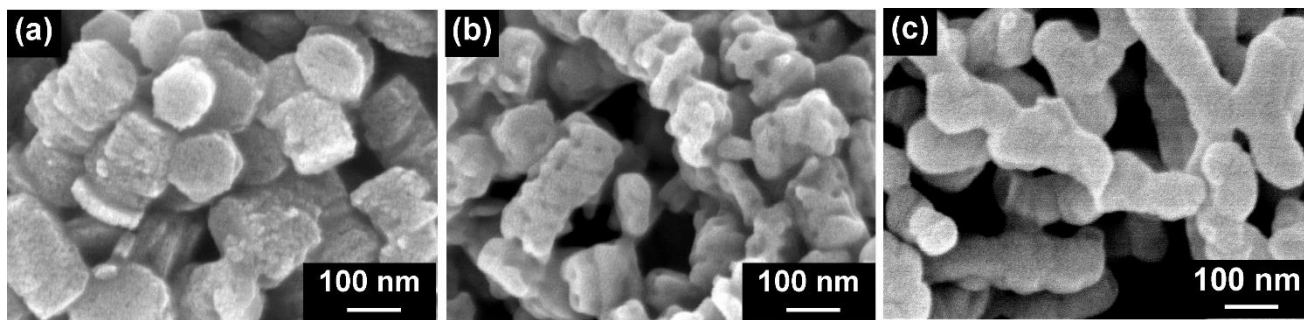


Figure S9. SEM images of the products achieved by calcination of Ni-Co-TEP particles at (a) 400 °C (Ni-Co-TEP-400), (b) 600 °C (Ni-Co-TEP-600), and (c) 800 °C (Ni-Co-TEP-800).

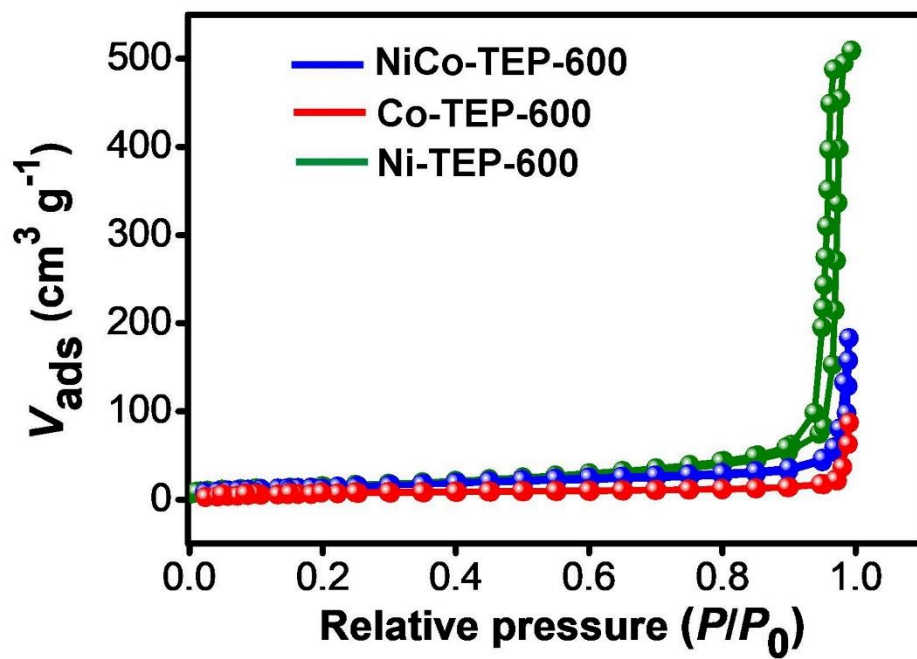


Figure S10. N_2 adsorption-desorption isotherms of Ni-TEP-600, Ni-Co-TEP-600, and Co-TEP-600.

Table S3. Comparison of the OER performance of the Ni-Co-TEP-600 catalyst with previously reported phosphate-based catalysts.

Catalyst	Electrolyte	η_{10} (mV)	Tafel slope (mV dec⁻¹)	Reference
Nanoplate-assembled chain-like Ni-Co phosphate particles	1.0 M KOH	320	68.0	This work
Cobalt phosphate plates	1.0 M KOH	350	68.0	1
Nickel phosphate plates	1.0 M KOH	374	85.4	1
Nickel-cobalt phosphate plates	1.0 M KOH	388	90.3	1
Nanotube-assembled Ni-Co hydrogen phosphate sheets	1,0 M KOH	320	84.0	2
Ordered mesoporous cobalt phosphate	1.0 M KOH	380	58.7	3
NaCo(PO ₃) ₃ with partially graphitized carbon	1.0 M KOH	340	76.0	4
Co ₂ P ₂ O ₇ nanowires	1.0 M KOH	359	54.1	5
Co ₂ P ₂ O ₇ nanobelts	1.0 M KOH	371	57.9	5
Co ₂ P ₂ O ₇ nanoleaves	1.0 M KOH	390	81.6	5
Co ₂ P ₂ O ₇ nanorhombuses	1.0 M KOH	424	119	5
Co ₃ (PO ₄) ₂ @N-doped carbon	1.0 M KOH	317	62.0	6
(Fe ₄ Co ₁)P ₂ O ₇ @N-C hybrid	1.0 M KOH	341	34.9	7
Flower-like Co-Zn phosphate	1.0 M KOH	382	83.2	8
Fe-Co phosphate nanosheets	1.0 M KOH	267	30.0	9

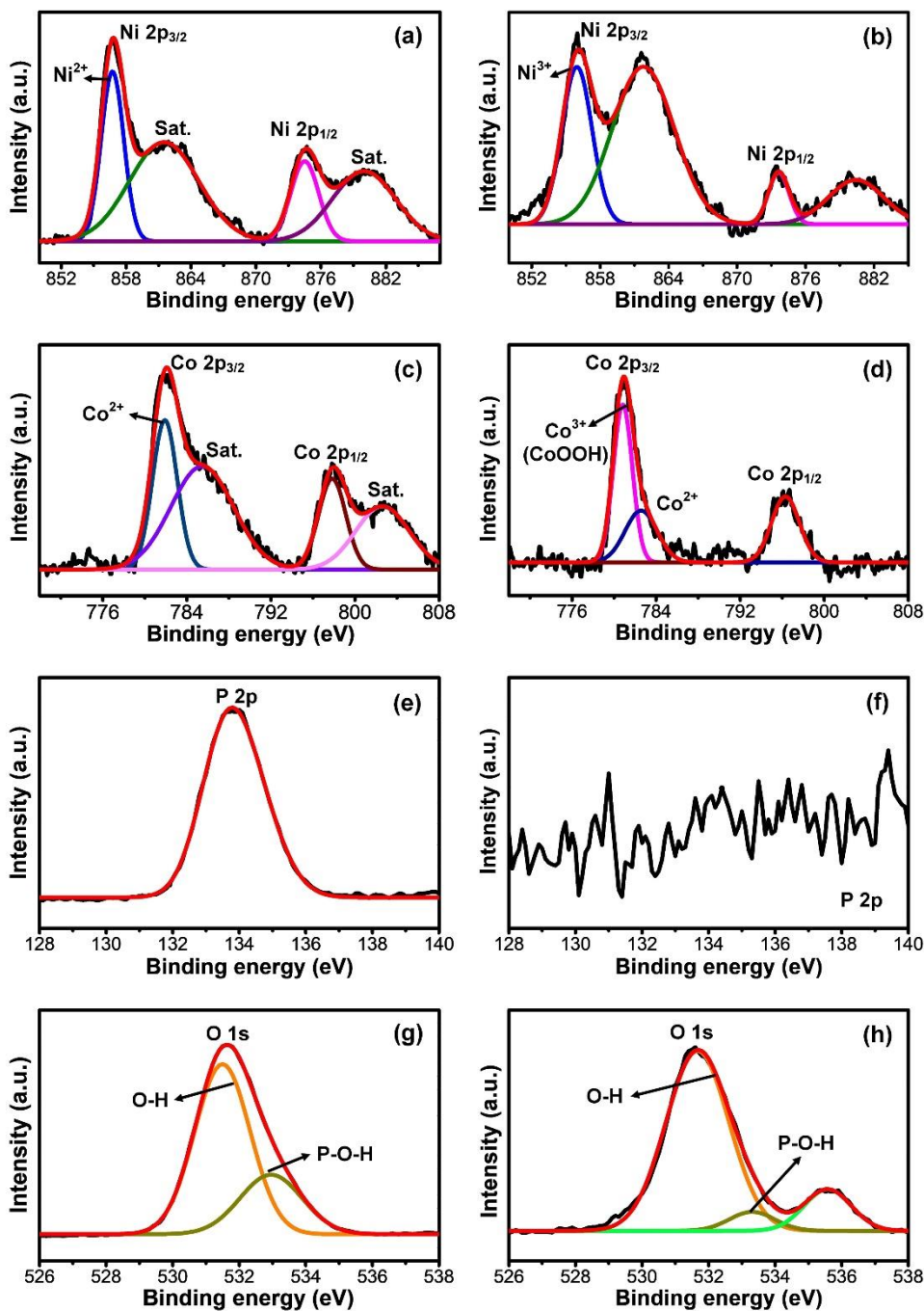


Figure S11. High-resolution Ni 2p spectra of Ni-Co-TEP-600 before (a) and after (b) the stability test for OER. High-resolution Co 2p spectra of Ni-Co-TEP-600 before (c) and after (d) the stability test for OER. High-resolution P 2p spectra of Ni-Co-TEP-600 before (e) and after (f) the stability test for OER. High-resolution O 1s spectra of Ni-Co-TEP-600 before (g) and after (h) the stability test for OER.

SI References

1. Bhanja, P.; Kim, Y.; Paul, B.; Lin, J.; Alshehri, S. M.; Ahamad, T.; Kaneti, Y. V.; Bhaumik, A.; Yamauchi, Y., Facile Synthesis of Nanoporous Transition Metal-Based Phosphates for Oxygen Evolution Reaction. *ChemCatChem* **2020**, *12*, 2091-2096.
2. Septiani, N. L. W.; Kaneti, Y. V.; Fathoni, K. B.; Guo, Y.; Ide, Y.; Yulianto, B.; Jiang, X.; Nugraha; Dipojono, H. K.; Golberg, D.; Yamauchi, Y., Tailorable Nanoarchitecturing of Bimetallic Nickel–Cobalt Hydrogen Phosphate via the Self-Weaving of Nanotubes for Efficient Oxygen Evolution. *J. Mater. Chem. A* **2020**, *8*, 3035-3047.
3. Pramanik, M.; Li, C.; Imura, M.; Malgras, V.; Kang, Y.-M.; Yamauchi, Y., Ordered Mesoporous Cobalt Phosphate with Crystallized Walls toward Highly Active Water Oxidation Electrocatalysts. *Small* **2016**, *12*, 1709-1715.
4. Gond, R.; Singh, D. K.; Eswaramoorthy, M.; Barpanda, P., Sodium Cobalt Metaphosphate as an Efficient Oxygen Evolution Reaction Catalyst in Alkaline Solution. *Angew. Chem. Int. Ed.* **2019**, *58*, 8330-8335.
5. Du, H.; Ai, W.; Zhao, Z. L.; Chen, Y.; Xu, X.; Zou, C.; Wu, L.; Su, L.; Nan, K.; Yu, T.; Li, C. M., Engineering Morphologies of Cobalt Pyrophosphates Nanostructures toward Greatly Enhanced Electrocatalytic Performance of Oxygen Evolution Reaction. *Small* **2018**, *14*, 1801068.
6. Yuan, C.-Z.; Jiang, Y.-F.; Wang, Z.; Xie, X.; Yang, Z.-K.; Yousaf, A. B.; Xu, A.-W., Cobalt Phosphate Nanoparticles Decorated with Nitrogen-Doped Carbon Layers as Highly Active and Stable Electrocatalysts for the Oxygen Evolution Reaction. *J. Mater. Chem. A* **2016**, *4*, 8155-8160.
7. Zhao, D.; Shao, Q.; Zhang, Y.; Huang, X., N-Doped Carbon Shelled Bimetallic Phosphates for Efficient Electrochemical Overall Water Splitting. *Nanoscale* **2018**, *10*, 22787-22791.
8. Qian, L.; Miao, Y., Nanosheet Organized Flower-Like Co/Zn Phosphate on Nickel Foam for Efficient Water Splitting in Both Acid and Basic Solutions. *Polyhedron* **2019**, *160*, 213-218.
9. Yin, D.; Jin, Z.; Liu, M.; Gao, T.; Yuan, H.; Xiao, D., Microwave-Assisted Synthesis of the Cobalt-Iron Phosphates Nanosheets as an Efficient Electrocatalyst for Water Oxidation. *Electrochem. Acta* **2018**, *260*, 420-429.